Ocean Dynamics (2026) 76:24
https://doi.org/10.1007/s10236-026-01782-y

Propagation patterns of swells generated by tropical cyclone Freddy and its coastal impacts along the Indian ocean rim

Roshyal Joy[1,2] · Remya P G[1] · B. Praveen Kumar[1] · R. S. Mahendra[1] · T. M. Balakrishnan Nair[1]

Received: 30 September 2025 / Accepted: 9 February 2026

Abstract
This study examines the swells generated by Tropical Cyclone (TC) Freddy, an exceptionally long-lived cyclone that traversed the southern Indian Ocean (SIO) westward during February 2023. The intensification and prolonged duration of severe TCs are anticipated to increase, making them a greater threat under future climate conditions. While swells are not the most intense sea conditions, these low frequency swells lead to coastal hazards such as erosion and flooding, hence understanding the TC trends and the effect along the coastlines is crucial. The modelling experiments are carried out using WAVEWATCH III (WW3). The analysis quantified TC 2023 Freddy–generated swell energy and revealed their ability to propagate across the basin, reaching the coasts of India, Sri Lanka, the Maldives, Lakshadweep, the Gulf region, and eastern Africa. Spectral evolution demonstrated how cyclone-forced wind seas transformed into dominant long-period swells, with nonlinear interactions amplifying low-frequency energy during cyclones peak intensity. Wave power density analysis further indicated that southern India and nearby island regions experienced the strongest swell impacts, with values reaching 0.5–2 kW/m. These findings highlight the far-reaching influence of long-lived cyclones on distant coasts and provide critical insights for anticipating coastal vulnerability and developing effective protection strategies under future climate scenarios.

Keywords Unstructured WAVEWATCH III · Non-linear wave-wave interactions · Wave power density · Swell propagation · Tropical cyclone Freddy · Wave modeling

1 Introduction

A tropical cyclone (TC) is a large-scale convective atmospheric system that generates intense wind fields, disturbing the ocean surface and producing high-energy waves. Globally, TCs (or hurricanes or typhoons) are characterised by sustained wind speeds exceeding ~ 33 m/s, with the most intense systems reaching ~ 50 m/s at peak intensity, and associated significant wave heights typically in the range of ~ 6–15 m, leading to extreme oceanic conditions (Grossmann-Matheson et al. 2024). These conditions severely impact navigation, coastal infrastructure, and can cause coastal flooding and beach erosion (Shimura et al. 2015; Tamizi and Young 2020; Ghanavati et al. 2023).

Apart from generating local wind-seas, TCs consist of a rotating low-pressure system surrounded by high wind fields that radiate waves outward from the storm centre. Long-period swell waves are typically formed due to resonance between the group velocity of waves and translational speed of the storm, especially when aligned with high wind speeds. These energetic swells can travel long distances with minimal energy loss, often retaining significant intensity comparable to that within the generation zone (Walsh et al. 2000; Ardhuin et al. 2009; Wu et al. 2024). When these low-frequency swells reach the coast, they can result in hazardous wave conditions (Tamizi and Young 2020; Davison et al. 2024).

In recent decades, global patterns of tropical cyclone activity have shown notable variability in frequency, intensity, and regional distribution, prompting increased scientific attention. Anthropogenic global warming has led to

Responsible Editor: Baba Mytheenkhan

✉ Remya P G
remya.pg@incois.gov.in

[1] Indian National Centre for Ocean Information Services (INCOIS), Ministry of Earth Scienes (MoES), Hyderabad, India

[2] Kerala University of Fisheries and Ocean Studies (KUFOS), Kochi, India

Published online: 23 February 2026

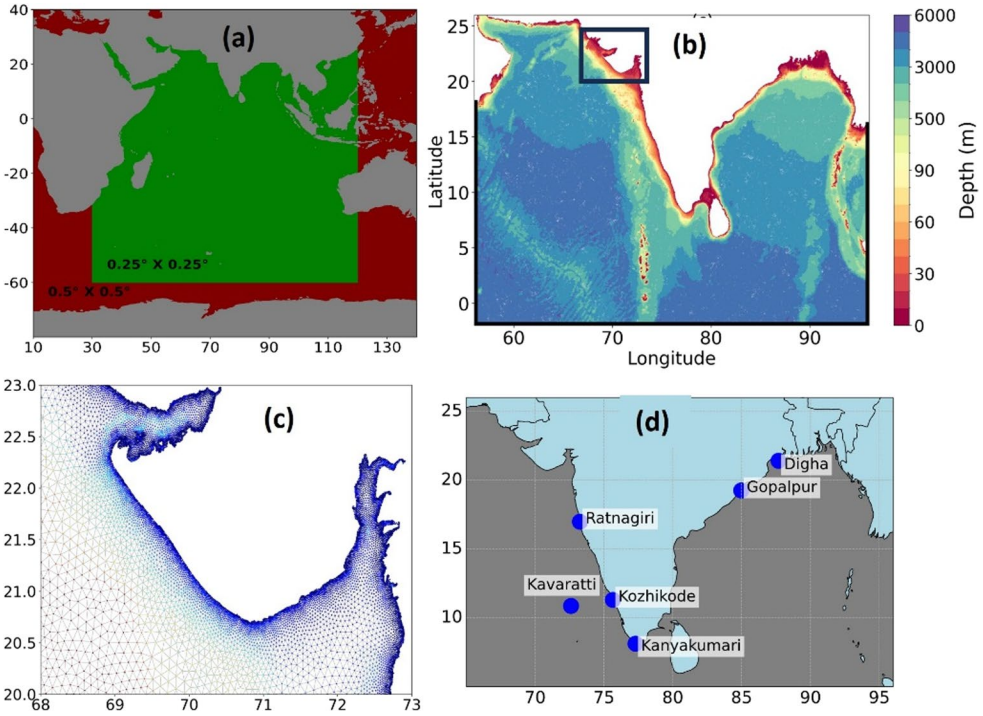

Fig. 1 Study area and WAVEWATCH III model domains: (**a**) multigrid global and IO setup; (**b**) unstructured NIO domain with open boundary (black line); (**c**) zoomed view of the unstructured mesh; and (**d**) wave buoy locations used in the study

increased Sea Surface Temperatures (SSTs), and combined with favourable atmospheric conditions, has contributed to rising TC frequency and intensity, resulting in large-scale losses and threats to human life (Peduzzi et al. 2012; Kossin et al. 2020; Klotzbach et al. 2022). Hence, understanding TC trends and their impacts along coastlines is crucial.

This is especially important for a country like India, with a coastline of about ~ 11,000 km spanning nine states. Understanding the impact of cyclone-induced waves along the Indian coast becomes indispensable. The North Indian Ocean (NIO) experiences tropical cyclones approximately in a ratio 3:1 annually—three in the Bay of Bengal (BoB) and one in the Arabian Sea (AS)—accounting for around 5% of global TCs (Singh 2010; Paul et al. 2022). However, recent decade exhibits significant changes in the nature of tropical cyclone in the NIO also in terms of increasing trend in the intensity, frequency, and duration (Deshpande et al. 2021; Sebastian and Behera 2015).

Another significant contributor to high wave conditions along the Indian coast is the swell from the Extra-Tropical Southern Indian Ocean (ETSIO). Various studies have analyzed the general propagation characteristics of these swells toward the NIO region (Bhowmick et al. 2011; Sabique et al. 2012; Samiksha et al. 2012; Remya et al. 2016; Zheng

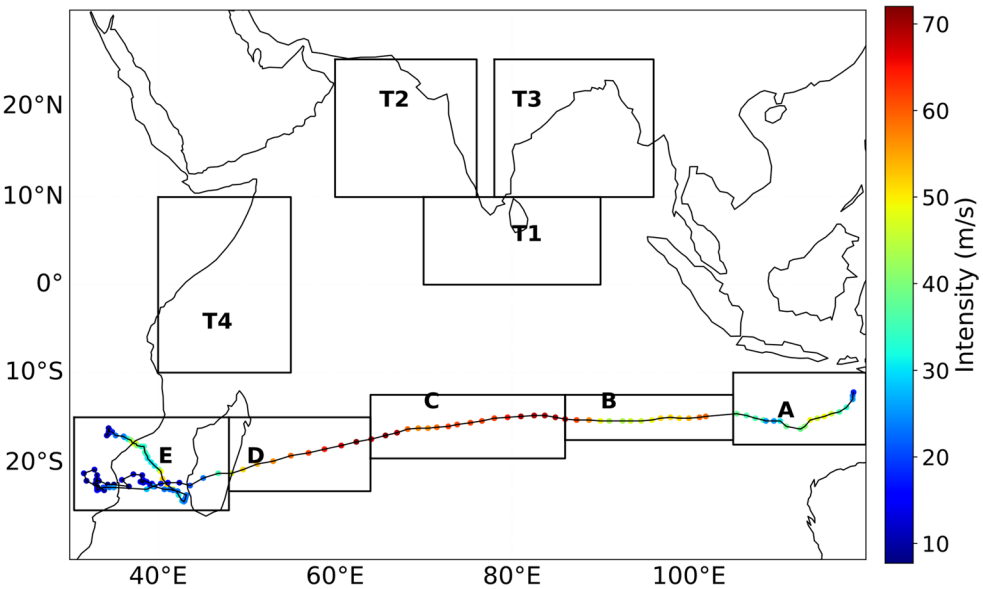

Fig. 2 Freddy cyclone track with intensity and focus areas chosen for the study

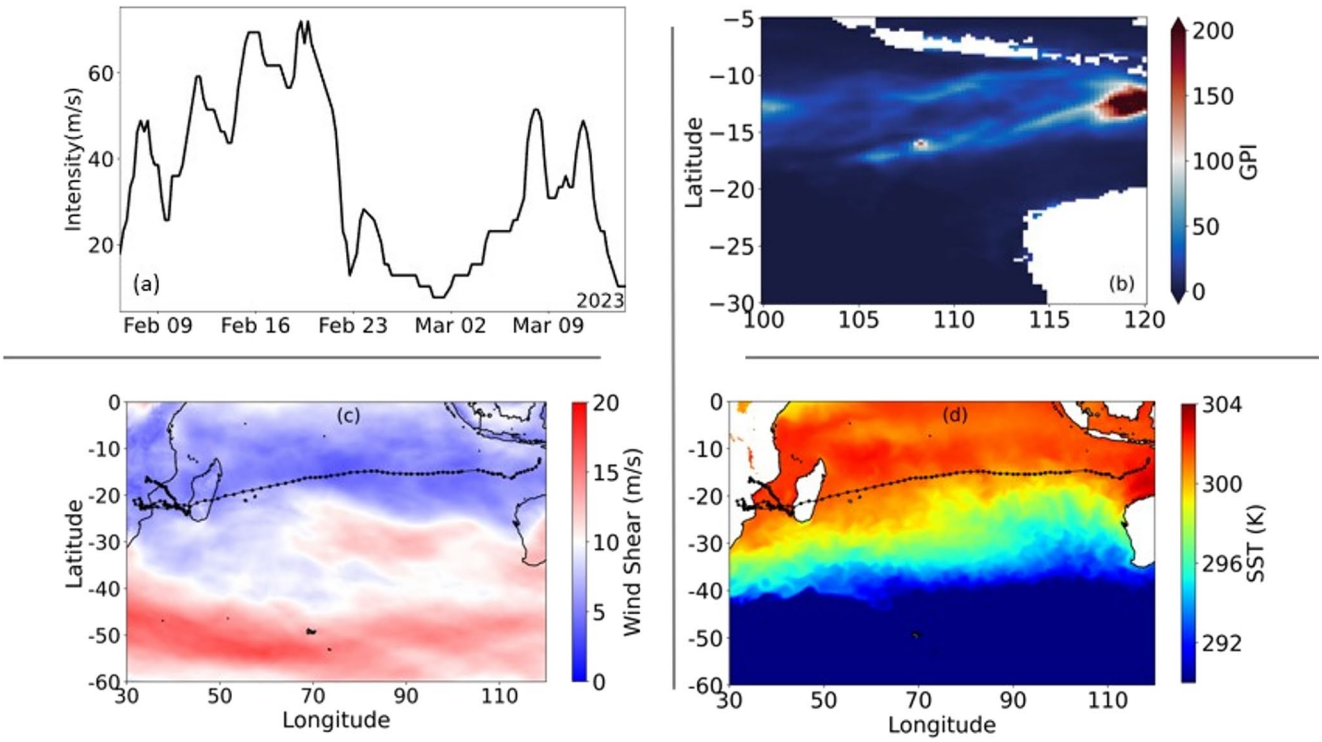

Fig. 3 (**a**) Temporal evolution of cyclone intensity; (**b**) Genesis Potential Index (GPI) averaged over the period from 00:00 UTC on 3 February to 12:00 UTC on 6 February; (**c**) vertical wind shear (m/s) averaged for February 2023; and (**d**) Sea Surface Temperature (SST, K) averaged for February 2023

et al. 2018; Sreelakshmi and Bhaskaran 2022). Extratropical cyclones originating between 50°S and 70°S (with additional activity between 30°S and 50°S) generate swell waves with typical lifespans of 3–5 days (Reboita et al. 2015). However, their contribution to Indian coastal wave conditions is significant. Yet, there have been no studies on the swell propagation characteristics due to wave fields from the TCs formed at the Tropical Southern Indian Ocean

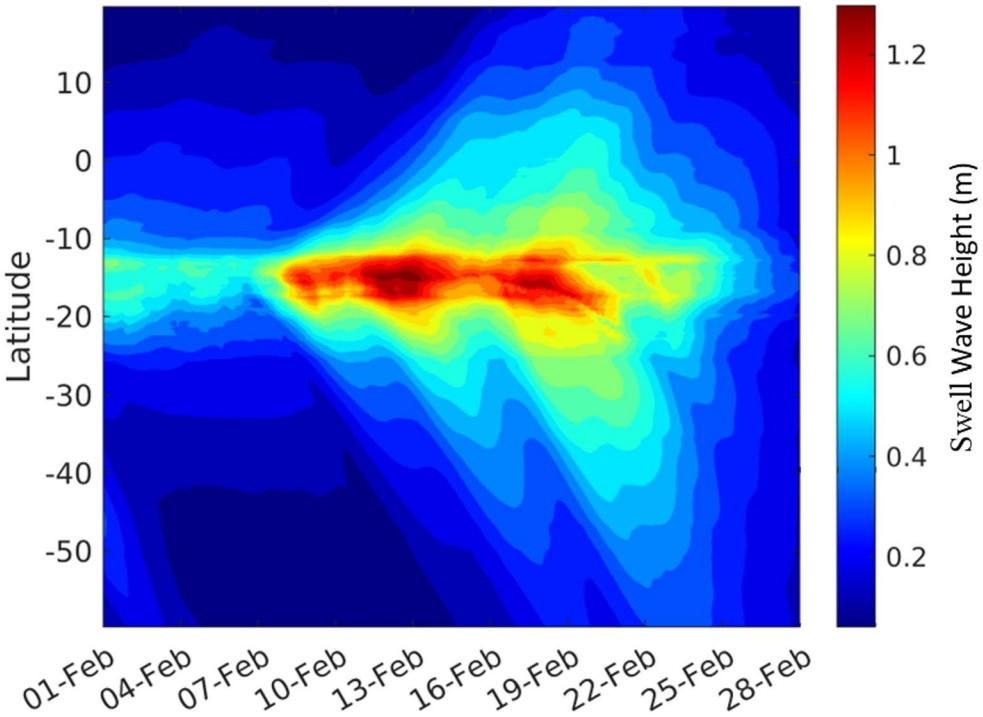

Fig. 4 Hovmöller diagram showing the zonal average of swell wave height (m) over the Indian Ocean [30°E–120°E]

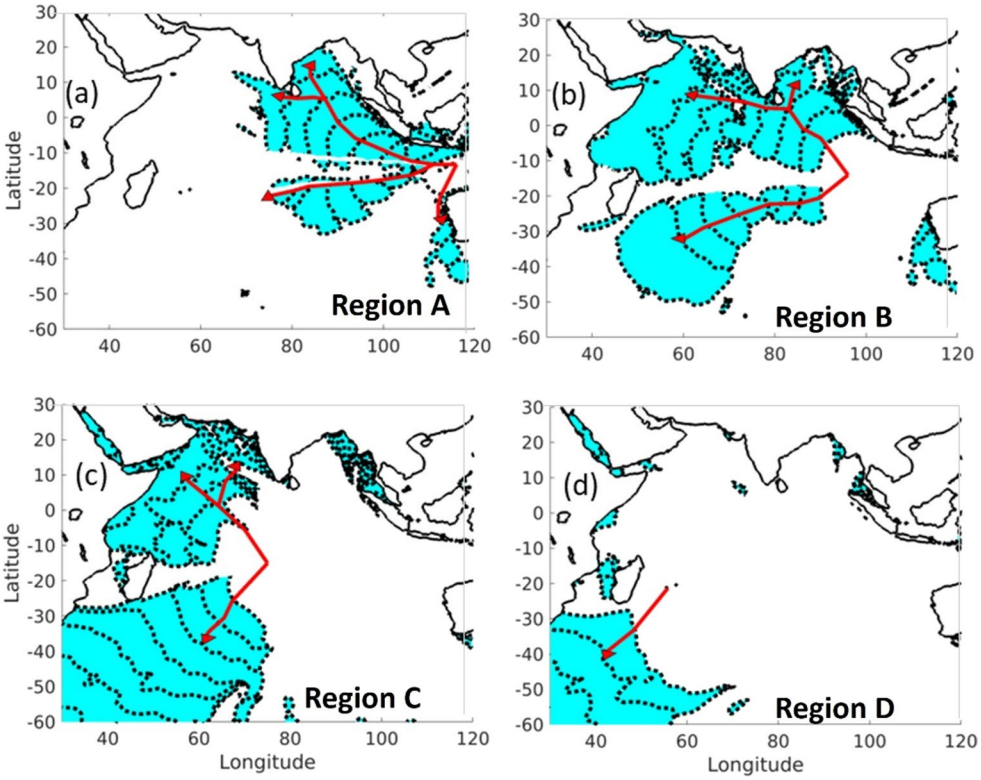

Fig. 5 Propagation routes of swell energy from (**a**) Region A; (**b**) Region B; (**c**) Region C; and (**d**) Region D

(TSIO) region. Hence understanding the swell propagation pattern due to TC wavefields and the degree of impact across the IO coasts is an overlooked area.

In this study, we focus on swells generated by Tropical Cyclone Freddy, a long-lived system that traversed the entire Indian Ocean westward in February 2023. This rare event is comparable to the tracks of TC Eline (February, 2000) and TC Hudah (March, 2000), both of which crossed the Southern Indian Ocean (SIO) and made multiple landfalls in Madagascar and Mozambique, causing significant coastal impacts. The growing threat of intense tropical cyclones remains a global concern. According to (Knutson et al. 2015), while the overall number of TCs may decline in a warmer late 21 st century, the average intensity and number of very severe cyclones are expected to increase.

Thus, gaining insights into the swell propagation patterns of TC Freddy is crucial. Although the most significant threats from such cyclones are typically to Madagascar and the eastern coasts of Africa, little research exists on how the wave fields from TC Freddy have propagated across the Indian Ocean and which regions of the Indian coast may have been affected. While swells may not represent the most extreme sea conditions, their low-frequency nature can lead to significant coastal hazards (Kumar et al. 2009). Even though there are numerous studies illustrating the swell propagation patterns along the IO (Zheng et al. 2018, 2022; Sreelakshmi and Bhaskaran 2023), there was no reference for the swell propagation route from a TC like Freddy. Thus analyzing the swell propagation patten from cyclone like TC Freddy helps for futuristic coastal protection during a similar situation. Hence this study investigates the swell propagation patterns and identifies the coastal areas which are prone to these swells.

Rest of the article is organized as follows: Sect. 2 describe data and methodology. Section 3 and Sect. 4 presents an overview of the TC Freddy, Sect. 5 evaluates the results and provides a discussion. Section 6 presents summary and conclusion of the study.

Table 1 Summary of swell arrival time and the affected regions along different target regions

Regions	Timing of Arrival Across Target Areas	Affected Regions
Region A	T1–168 h T2–192 h T3–192 h	Indonesian Archipelago, Sumatra Islands, Srilanka, India
Region B	T1–96 h T2–120 h T3- 120 h T4–192 h	Sumatra Islands, Andaman & Nicobar Islands, Myanmar, India, Gulf of Aden, Oman, Africa, Madagascar.
Region C	T2–72 h T4–96 h	India (west coast), Gulf region, Africa, Madagascar
Region D	T4–24 h	Africa, Madagasacar

Fig. 6 Non-linear wave-wave interactions and 1D-spectra along the cyclone track (**a**) 6th Feb 00:00, (**b**) 6th Feb 12:00, (**c**) 6th Feb 18:00, (**d**) 7th Feb 00:00

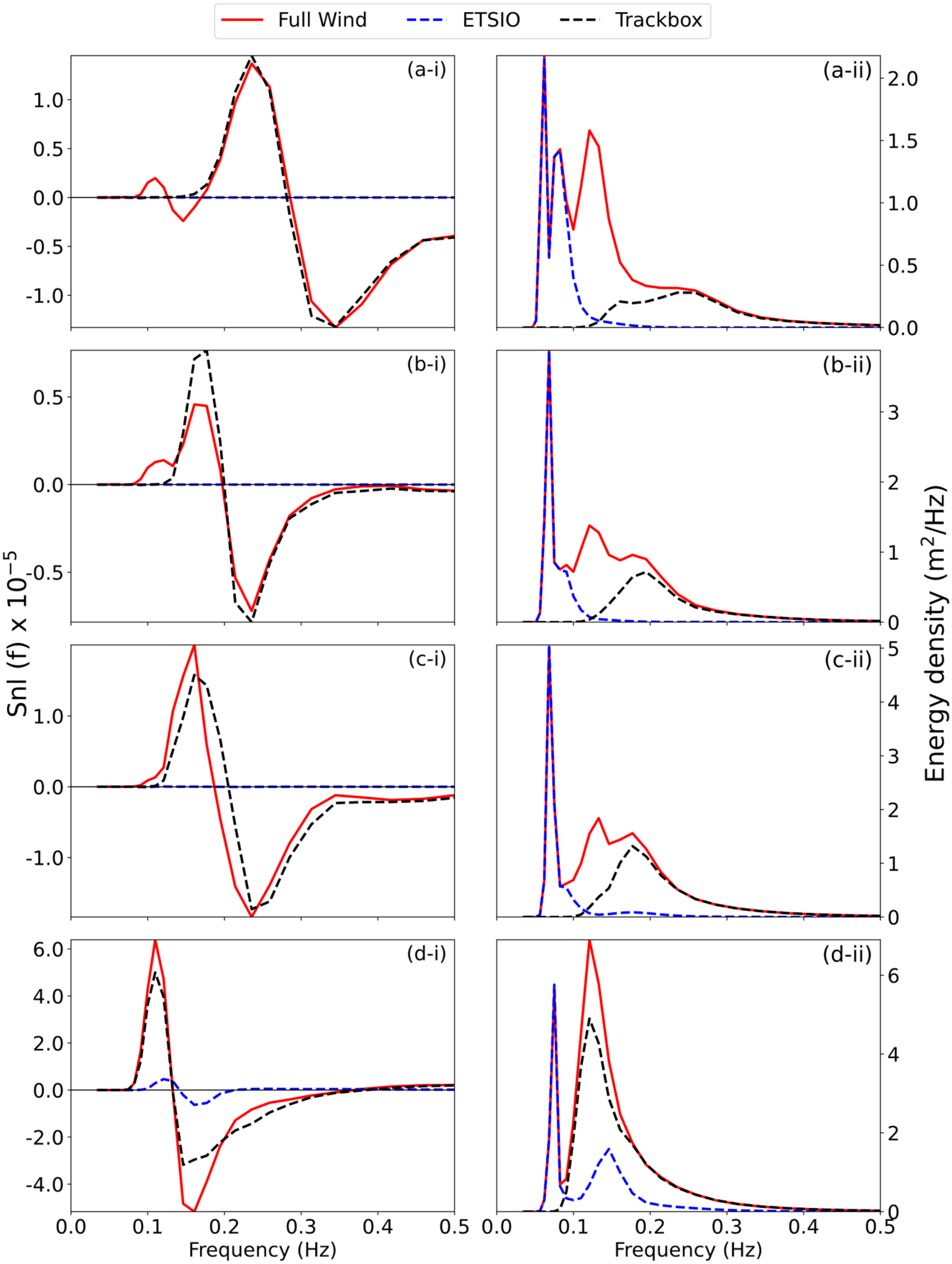
Full Wind
ETSIO
Trackbox
(a-i)
(a-ii)
(b-i)
(b-ii)
(c-i)
(c-ii)
(d-i)
(d-ii)
Snl (f) x 10^{-5}
Energy density (m^2/Hz)
Frequency (Hz)
Frequency (Hz)

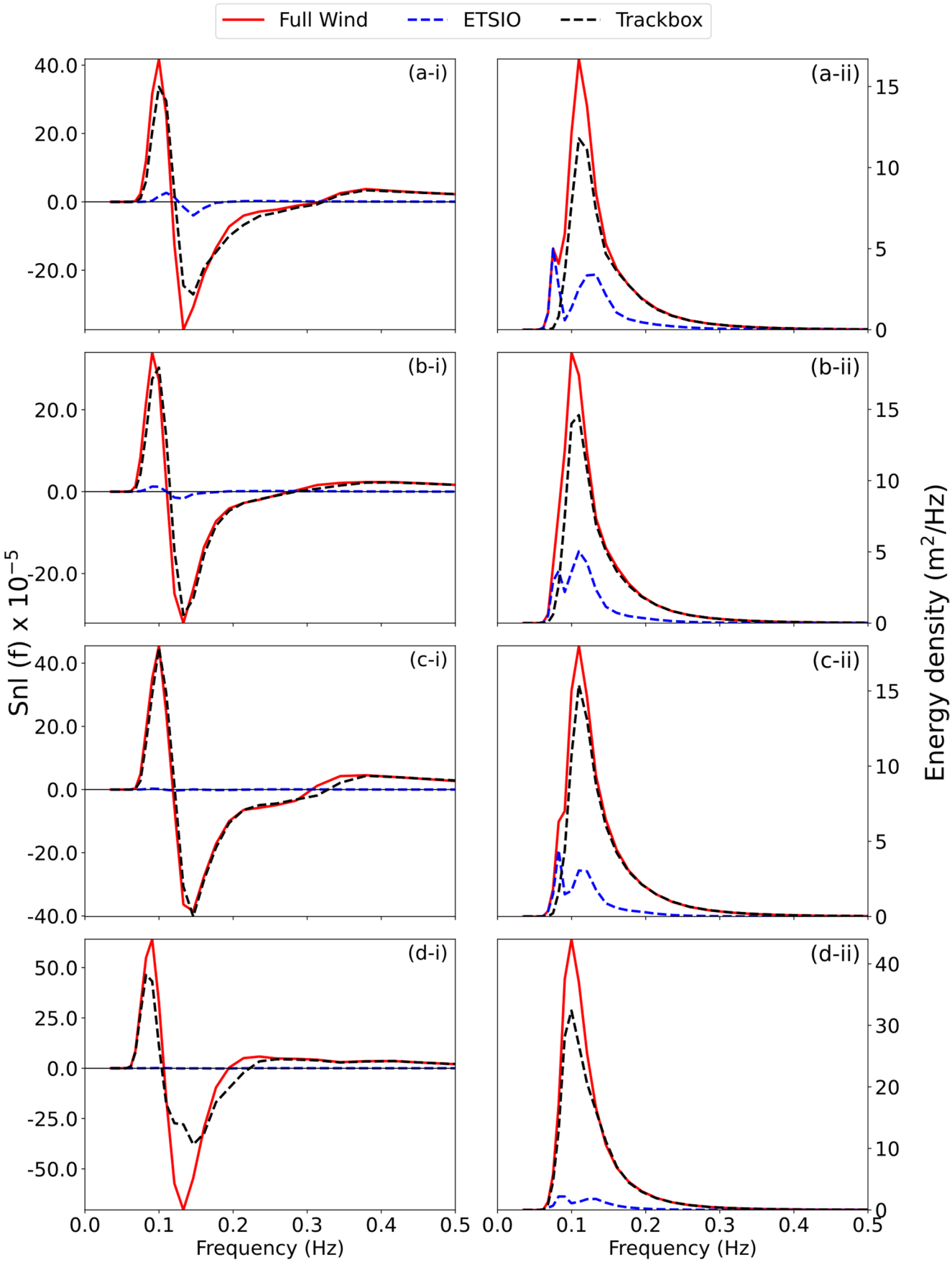
Full Wind
ETSIO
Trackbox
(a-i)
(a-ii)
(b-i)
(b-ii)
(c-i)
(c-ii)
(d-i)
(d-ii)
Snl (f) x 10^{-5}
Energy density (m^2/Hz)
Frequency (Hz)
Frequency (Hz)

Fig. 7 Non-linear wave-wave interactions and 1D-spectra along the cyclone track (**a**) 7th Feb 06:00, (**b**) 7th Feb 12:00, (**c**) 7th Feb 18:00, (**d**) 8th Feb 06:00

2 Data and methodology

2.1 Model used

The present study employs the third-generation numerical wave model WAVEWATCH III (WW3) developed by NOAA/NCEP (WWIII Development Group, 2016). The model solves the general wave action balance equation, which accounts for all relevant physical processes such as wave generation, propagation, nonlinear interactions and dissipation (Tolman 2009). The conservative terms, including local rate of change and spatial and spectral propagation, are balanced by non-conservative source and sink terms. In deep water, the net source term comprises three components: wind–wave interaction (S_{in}), nonlinear wave–wave interactions (S_{nl}), and dissipation due to whitecapping (S_{ds}). In shallow water, additional processes such as wave–bottom interaction (Sbot), depth-induced wave breaking (S_{db}), and triad wave–wave interactions (S_{tr}) are also considered.

In this study, two WW3 model configurations are used. First, a regular multi-grid setup is implemented, consisting of a global grid [0°–360°, 80°S–80°N] with 0.5° resolution and an Indian Ocean grid [30°E–120°E, 60°S–30°N] with 0.25° resolution (Fig. 1a), to analyze the propagation of waves from TC Freddy over the Indian Ocean region. Second, an unstructured WW3 configuration with spatial resolution varying from 1 to 10 km is developed for the NIO region [56°E–96°E, 2°S–26°N] to examine the coastal impact of TC-generated swells. These high-resolution grids are more effective for resolving coastal processes than coarser grids.

The unstructured grid for the NIO region is generated using OceanMesh2D, a MATLAB-based software for two-dimensional unstructured mesh generation in coastal ocean modelling (Roberts et al. 2019). INCOIS bathymetry data with a resolution of 200 m, which combines NHO survey data along the coasts with GEBCO-30s data is used for depth values in the coastal model (Ramakrishnan et al. 2022). Boundary spectral data for the NIO grid are derived from the 0.25° Indian Ocean grid (Fig. 1). The model employs the ST4 package for wind input and dissipation parameterizations (Raj et al. 2023), while bottom friction is parameterized using the JONSWAP formulation (Hasselmann et al. 1973).

Nonlinear wave–wave interactions are modeled using the Discrete Interaction Approximation (DIA). Quadruplet interactions represent nonlinear resonant processes in which four wave components exchange energy and momentum while conserving both quantities, thereby redistributing energy across different frequencies and directions within the wave spectrum. Two wave components, $k_1$and k_2, can exchange energy efficiently only in the presence of two additional components, k_3 and k_4, that satisfy the resonance conditions (Hasselmann 1963). Energy input from the wind occurs primarily near the spectral peak and mid-range frequencies, while dissipation due to whitecapping predominantly affects the higher-frequency components. The quadruplet interactions redistribute energy across the spectrum, promoting a more uniform distribution over wavenumber space. This process acts as a stabilizing mechanism and drives the wave spectrum toward the JONSWAP equilibrium shape (Hasselmann et al. 1973; Susilo et al. 2017).

As we know that the waves reaching the coast area is a combination of wind waves and swells, so here to understand how the swells generated from the TC Freddy along with ETSIO swells are affecting the NIO region, we carried out three different model experiments with three different model forcings. Initially with full wind fields in the IO regions (WW3F). Secondly, wind forcing was given along the TC tracks only hereafter called as WW3TC to understand the swell propagation from the TC Freddy. Lastly, we forced the model with wind only in the TSIO region to quantify the ETSIO swell contribution (WW3SI).

2.2 Data used

In this study, NCMRWF wind fields with a spatial resolution of 0.125° are used as model forcing. The National Centre for Medium-Range Weather Forecasting (NCMRWF) uses a Numerical Weather Prediction (NWP) system built on the NCMRWF Unified Model (NCUM). The NWP model uses global meteorological data from both conventional and satellite sources, with wind analyses available at 00, 06, 12, and 18 UTC.

The best-track data for Freddy is obtained from the International Best Track Archive for Climate Stewardship (IBTrACS-WMO) v4 dataset. The ERA-5 reanalysis dataset of 0.25-deg resolution and a temporal resolution of 3 h is used for SST, Air-temperature, Humidity, wind velocity etc. (Hersbach et al. 2020). Model validation was performed with the help of wave buoys from the ESSO-INCOIS WAMAN buoy network (Balakrishnan et al. 2025) (Fig. 1d).

2.3 Methodology

To better understand the TC Freddy evolutions an analysis of the initial conditions of the TC is carried out based on the Genesis Potential Index (GPI), an empirical formulation used to analyze the influence of these large-scale environmental factors developed by (Camargo et al. 2007).

$$GPI = \left(\frac{H}{50}\right)^3 \times \left|10^5\eta\right|^{\frac{3}{2}} \times (1 + 0.1V_{shear})^{-2} \times \left(\frac{V_{pot}}{70}\right)^3$$

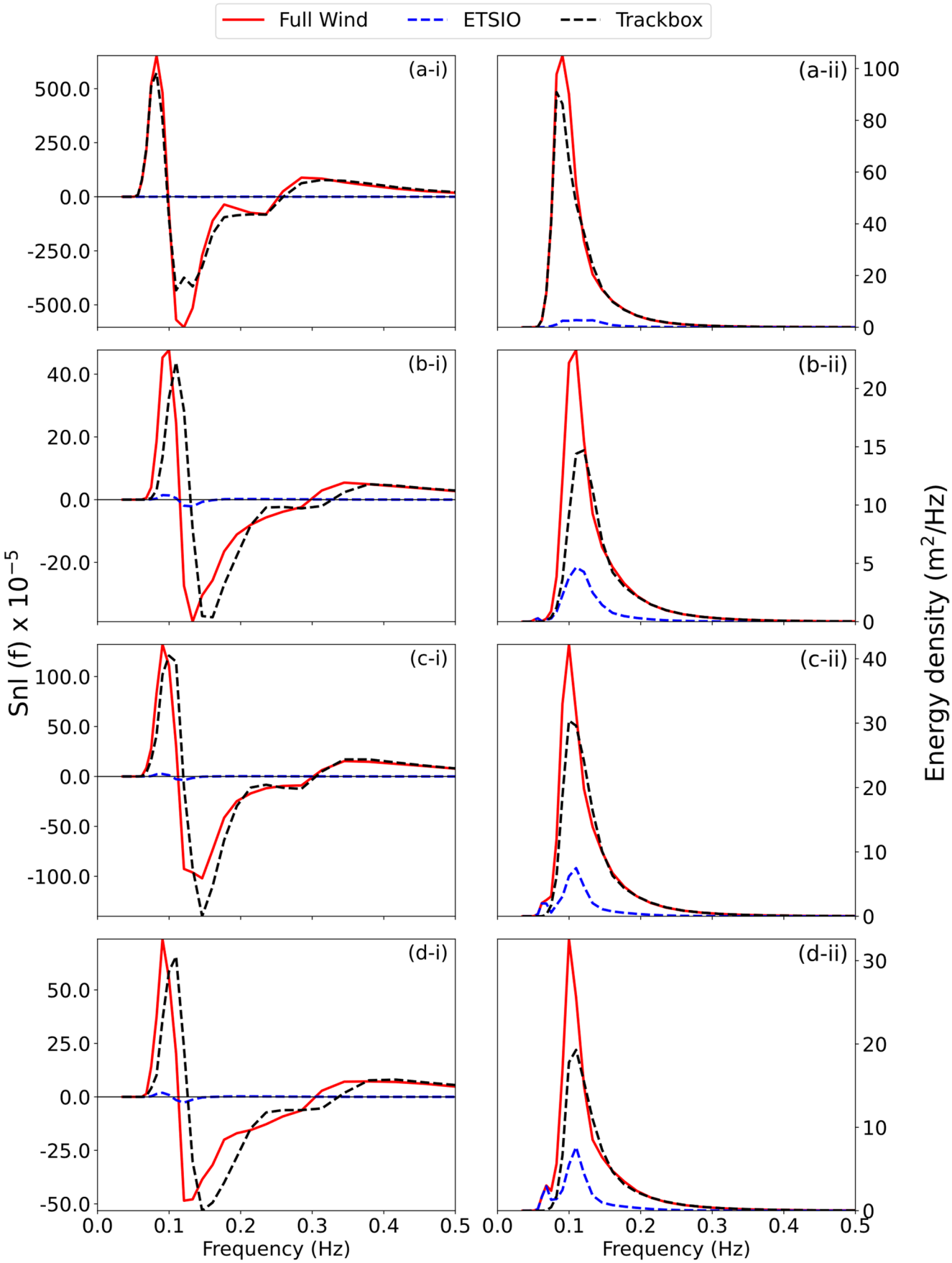
Full Wind
ETSIO
Trackbox
(a-i)
(a-ii)
(b-i)
(b-ii)
(c-i)
(c-ii)
(d-i)
(d-ii)
Snl (f) x 10^{-5}
Energy density (m^2/Hz)
Frequency (Hz)
Frequency (Hz)

Fig. 8 Non-linear wave-wave interactions and 1D-spectra along the cyclone track (**a**) 9th Feb 00:00, (**b**) 9th Feb 12:00, (**c**) 10th Feb 12:00, (**d**) 10th Feb 18:00

The symbols represent the following: η is the absolute vorticity at 850 hPa in s^{-1}, H is relative humidity at 600 hPa in %, and Vshear is the vertical shear magnitude (m/s) between 850 hPa and 200 hPa, Vpot is maximum TC Potential Intensity (PI) (ms − 1) (Emanuel 1988; Bister and Emanuel 2002).

The swell propagation patterns from the TC Freddy along the IO is done based on the method explained in (Zheng et al. 2018). The entire swell track is divided into five regions starting from the initiation period to the landfall region as shown in Fig. 2. The regions are divided as follows A [105°E-120°E; 18°S-10°S], B [86°E-105°E; 17.5°S-12.5°S], C [64°E-86°E; 19.5°S-12.5°S], D [48°E-64°E; 23°S-15°S], E [30°E-48°E; 25°S-15°S] etc. The Swell Index (SWI) for each region is determined based on the average Wave Power Density (WPD),

$$WPD = \frac{\rho g^2}{64\pi} H_s^2 T_e = 0.49 H_s^2 T_e$$

Where H_s is the swell wave height in meters, T_e is the energy period in seconds, ρ is the sea water mass density (ρ =1028Kg/ m^3), g is the gravitational acceleration ($g = 9.8m/s^2$), the WPD is calculated every three hourly. The leading correlation coefficients of the terminal area with respect to the SWI in each region is done to determine the propagation pattern of the swells along the IO and in the target regions as shown in Fig. (2). The target regions are T1 [70°E-90°E; 0°N-10°N], T2 [60°E-76°E; 10°N-25°N], T3 [78°E-96°E; 10°N-25°N], T4 [40°E-55°E; 10°S-10°N].

The rate at which swell energy attenuates during its propagation from the source region to the destination is calculated as follows:

$$d_{r(t)} = \frac{WPD_{s(t)} - WPD_{e(t+n)}}{WPD_{s(t)}} \times 100\%$$

where, $d_{r(t)}$ represents the attenuation rate of swell energy at a given time t, $WPD_{s(t)}$ denote the swell wave power density (kW/m) at time t in the source region, and $WPD_{e(t+n)}$ refers to the swell wave power density in the terminal area after a lag of n days from the source.

3 Tropical cyclone Freddy

The TC Freddy is the longest active cyclone with a duration of 36 days from 4th February 2023 to 14th March 2023.Track of TC Freddy with intensity is shown in Fig. 2. A depression originated south of Indonesian Archipelago on 4th February which then developed into a TC on 6th February 1200 UTC, it moved westwards and moved across the open ocean. As it moved westward it underwent rapid intensification multiple times and after attaining its highest intensity, the cyclone advanced toward the northern Mascarene Islands, making the first landfall near Mananjary, Madagascar, on February 21. As it moved across Madagascar, the cyclone weakened further but regained strength after entering the Mozambique Channel, intensifying before making its second landfall near Vilanculos, Mozambique, on February 24. Even after crossing Mozambique, the cyclone persisted for several days causing rainfall and re-entered the channel on March 1, it then redeveloped as a tropical system and traveled along the coast of Madagascar. Before making its final landfall near Quelimane, Mozambique, on March 11, Freddy intensified again and upon moving inland, it lost strength rapidly and dissipated by March 14. The TC Freddy is second in terms of accumulated cyclone energy by World Meteorological Organization (WMO) reports and the cyclone traversed from east to west throughout the SIO as shown in Fig. 2.

4 Role of ocean–atmosphere interactions in sustaining TC Freddy

The life cycle of a tropical cyclone begins with the formation of an environment that has the necessary thermodynamic conditions for development of a cyclone to form are explained by (Gray 1975; Briegel 1997; Wu et al. 2020) are high sea surface temperature, high mid tropospheric humidity, weak vertical wind shear etc. From the average conditions during the period of 3rd February to 6th February, it is evident from the high GPI values around the genesis region that the met-oceanic conditions were favourable for the development of the cyclone (Fig. 3). The cyclone persisted for 36 days, a recent study by (Perry et al. 2024) has examined in detail the factors which contributed to the sustenance of the cyclone. According to the study, the Mascarene High (MH) exerted a dominant influence by steering Freddy westward through strong easterly winds, effectively preventing it from recurving. Also, the presence of TC Dingani led to a split in the MH, increasing steering flow and acting as a moisture conveyor that helped sustain TC Freddy's convective structure and intensity. Moreover, throughout the entire period, as indicated by Fig. 3c and d, conditions were favourable for cyclone growth, with sea surface temperatures in the range of 27–29°C and weak Vertical Wind Shear (VWS) in m/s (Sebastian and Behera 2015). A few cyclones reach eastern Africa, mainly because of the challenging topography and dry conditions. In this case the movement of TC Freddy in the Mozambique Channel was primarily guided by strong easterly steering flow associated with the MH

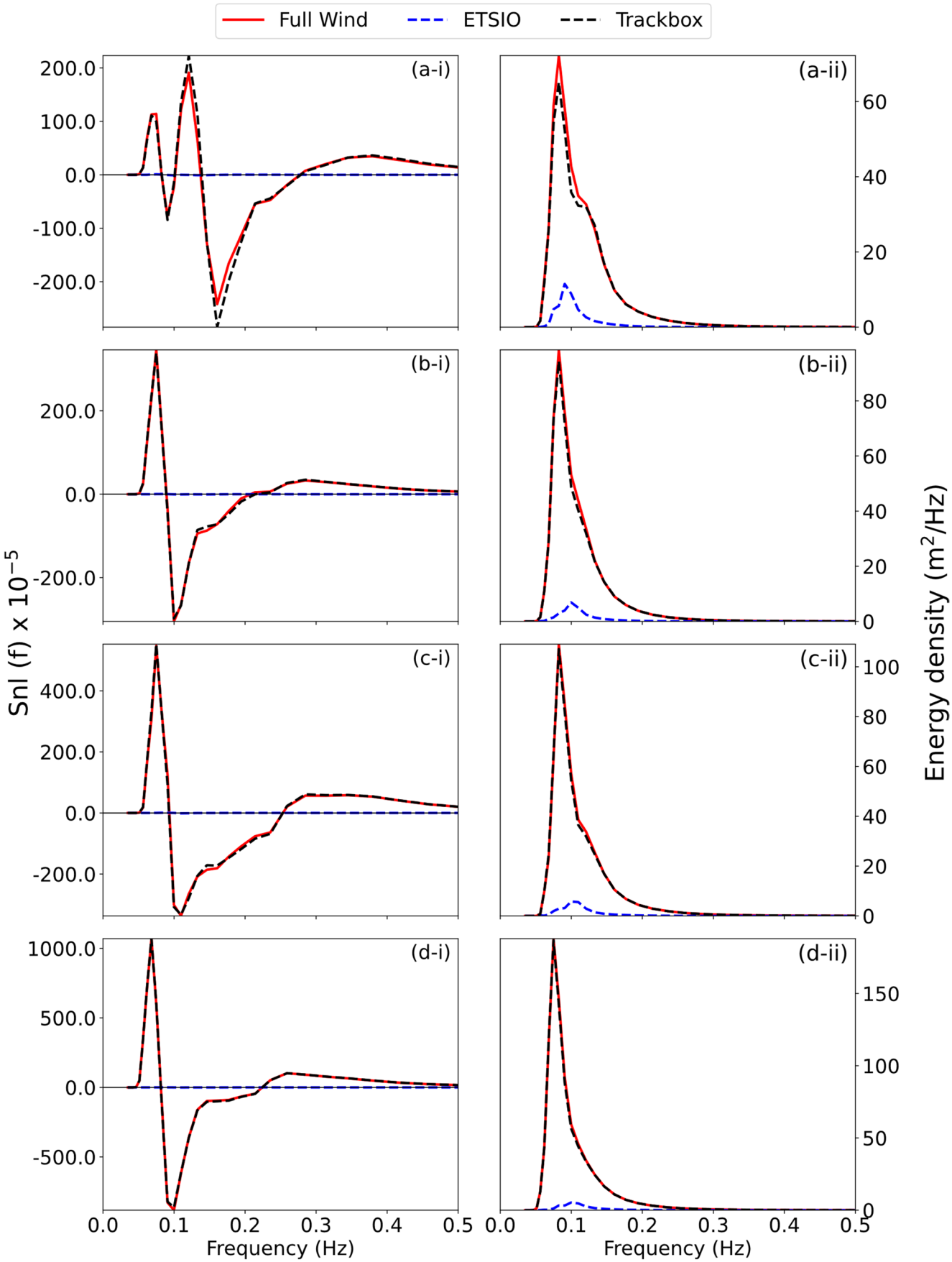
Full Wind
ETSIO
Trackbox
(a-i)
(a-ii)
(b-i)
(b-ii)
(c-i)
(c-ii)
(d-i)
(d-ii)
Snl (f) x 10^{-5}
Energy density (m^2/Hz)
Frequency (Hz)
Frequency (Hz)

Fig. 9 Non-linear wave-wave interactions and 1D-spectra along the cyclone track (**a**) 18th Feb 06:00, (**b**) 18th Feb 18:00, (**c**) 19th Feb 06:00, (**d**) 19th Feb 12:00

east of Madagascar, which acted as a barrier and directed the cyclone westward. It gained strength over the warm Mozambique Channel waters, made a brief landfall in southern Madagascar, but was deflected by an upper ridge, forcing it back to sea, where it re-intensified before hitting central Mozambique. The high-pressure systems supported Freddy through moisture convection retain strength over land and during its re-entry into the Mozambique Channel ultimately guiding it to its final landfall in central Mozambique (Perry et al. 2024; Ussalu and Manjate 2024).

5 Result and discussions

5.1 TC Freddy generated swell propagation pattern

The primary focus of this study is to understand how surface wave fields generated by a long-lived TC like Freddy propagated across the IO and impacted coastal areas during its east-to-west movement. Figure 4 shows the time-latitude Hovmöller diagram of swell wave heights for the IO region, derived from the WW3TC simulation, indicating how swells generated by the TC alone traversed the basin. The analysis clearly shows that the swell waves produced during the TC period were distributed across both the NIO and SIO regions. The zonal average of swells propagated into the NIO shows relatively low heights (<0.5 m). To further investigate the propagation across the IO, a swell propagation track was derived based on the correlation between the SWI in each region.

Figure 5a illustrates the swell propagation pattern from region A (Fig. 2), where the TC remained for 3 days (6–9 February). This region represents the generation zone of TC Freddy. As the cyclone moved westward, its intensity peaked at 48 m/s before weakening to 25 m/s. From region A, swells propagated in two main directions: one towards the northwest (NW) and the other towards the southwest (SW). The SW-propagating swells were directed towards the SIO, while the NW-propagating swells reached areas such as the Indonesian Archipelago, including Sumatra and Java. These swells reached region T1 by 168 h. Upon approaching the southern coasts of India and Sri Lanka, the swell field split into two branches: one towards the eastern coast of India and the other towards the western coast. These swells reached region T3 in about 192 h. Swells from region A had minimal influence on region T2. A smaller portion of the swell energy from region A also reached the western coasts of Australia.

Figure 5b illustrates the swell propagation from region B (Fig. 2). In this region, the cyclone intensified to a maximum of about 59 m/s before decreasing slightly to ~40 m/s. The swells generated followed two dominant directions: NW and SW, similar to those from region A. The SW component propagated towards the SIO regions, while the NW component advanced towards the Sumatra coast, the Andaman and Nicobar Islands, and eastern areas such as Myanmar. By ~96 h, the NW swells reached the southern NIO. Near the southern tip of India and Sri Lanka, the NW branch split into two: one moving north-eastward towards the eastern coast of India and the other north-westward towards the western coast. The swells arrived at the west coast (region T3) by ~120 h and subsequently extended towards the Gulf of Aden and the Oman coast, reaching them by ~192 h. By this time, the swells also propagated as far as the eastern African coast (region T4) and Madagascar.

Figure 5c presents the swell patterns from region C (Fig. 2). As the cyclone progressed westward through this region, it reached a maximum intensity of ~69 m/s. The swells again split into two dominant branches: the SW component propagated into the western IO, while the NW component extended towards the western Asian coasts, the Gulf region, eastern Africa, and Madagascar. These swells reached their farthest extent within ~96 h.

Figure 5d shows the swell propagation from region D (Fig. 2). Here, the cyclone reached a peak intensity of ~72 m/s before gradually weakening as TC Freddy made its first landfall. The swells generated from this region propagated towards the Madagascar coast, while a significant portion spread south-westward into the western IO.

Table 1 shows the summary of the swell arrival time and the affected regions from Regions A to D. Region E exhibited no significant swell propagation pattern during the passage of TC Freddy.

5.2 Swell modulations- spectral analysis

To better understand the role of wind forcing in swell generation and interaction, three different modelling experiments were conducted. In the first experiment, the full wind field was used, representing the most realistic condition with contributions from both the TC and the background wind field. This setup captures the combined effects of cyclone-generated wind seas, local wind sea swell interactions, and remotely generated swells propagating into the basin.

In the second experiment, winds were restricted to the track box alone, i.e., the immediate vicinity of the cyclone. This isolates the influence of the TC wind forcing, allowing the assessment swell generation and evolution directly

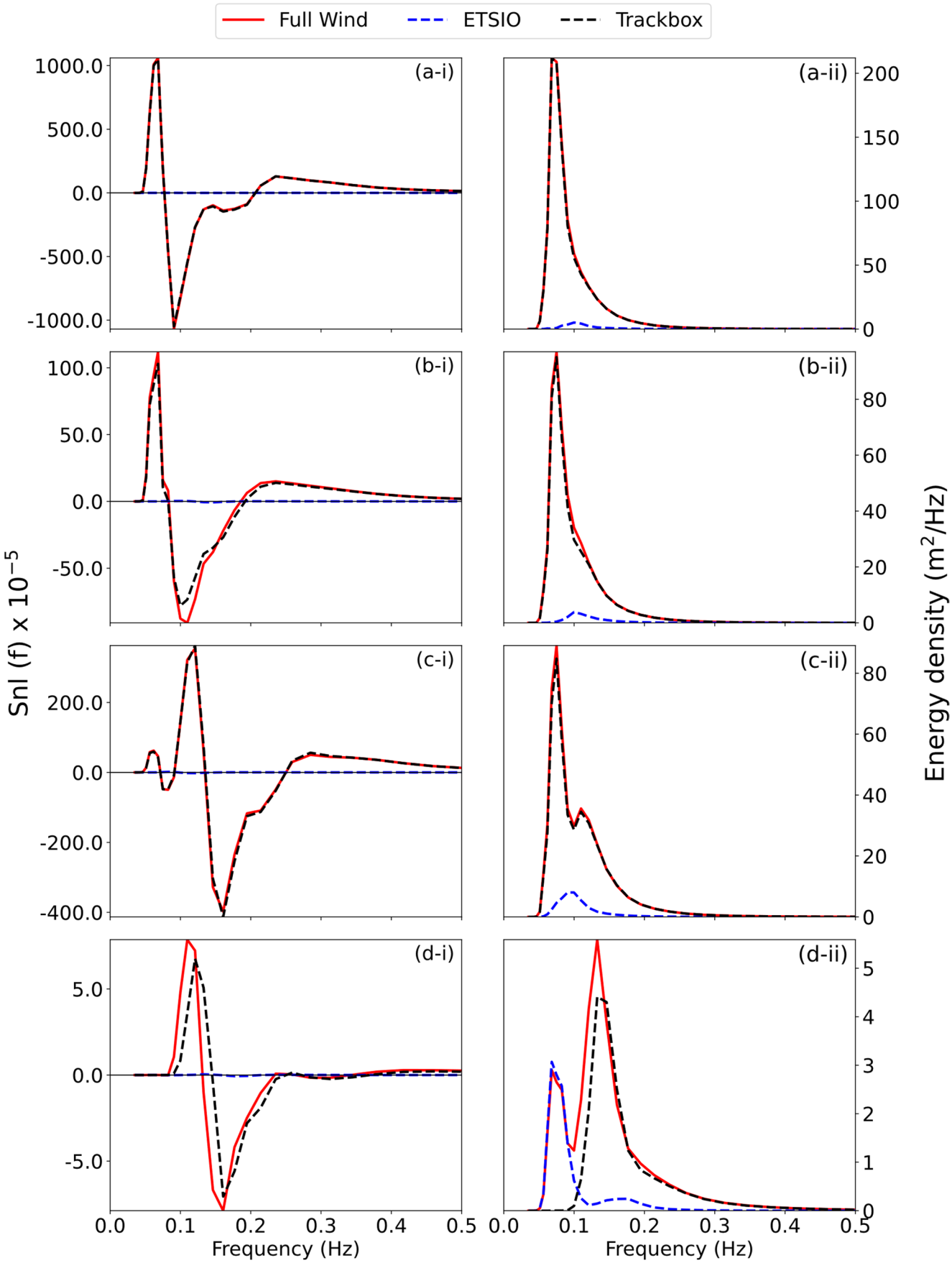
Full Wind
ETSIO
Trackbox
(a-i)
(a-ii)
(b-i)
(b-ii)
(c-i)
(c-ii)
(d-i)
(d-ii)
Snl (f) x 10^{-5}
Energy density (m^2/Hz)
Frequency (Hz)
Frequency (Hz)

Fig. 10 Non-linear wave-wave interactions and 1D-spectra along the cyclone track (**a**) 19th Feb 18:00, (**b**) 20th Feb 06:00, (**c**) 21 st Feb 12:00, (**d**) 22nd Feb 18:00

under the cyclone without interference from the broader background wind field.

The third experiment considered winds only in the ETSIO region, thereby excluding contributions from the NIO and other surrounding areas. This configuration highlights the role of ETSIO winds in generating long-period swells and their interaction with TC-generated waves.

Comparison of the wave spectra from these three experiments will give clarity on the relative influence of local TC winds, remote background winds, and ETSIO winds. This analysis offers insight into how cyclone-generated swells interact with swells originating from the ETSIO region and with one another, as well as how nonlinear processes redistribute energy across different frequency bands under varying forcing scenarios.

In this section, we analyse the One-Dimensional (1D) energy spectra and the S_{nl}(quadruplet/nonlinear wave–wave interaction) terms along the cyclone track to examine swell–swell interactions using the three model experiments described earlier. Waves in the TSIO generally consist of locally generated wind-sea and swells propagating from the ETSIO. The complex ocean wave field is better analysed using wave spectra, as spectral representation incorporates frequency, direction, and energy information. The 1D energy spectra may be double-peaked (bimodal), with a low-frequency swell peak and a high-frequency wind-sea peak (or two swell peaks), or single-peaked (unimodal), representing a single swell or wind-sea system in the TSIO.

Across Figs. 6, 7, 8, 9 and 10 the one-dimensional wave spectra (energy density) and S_{nl} panels show a consistent evolution as the cyclone develops, matures and makes landfall. Early stage (Fig. 6) shows a clear bimodal spectra i.e., a high-frequency wind-sea peak and a low-frequency swell peak where S_{nl} shows active exchanges that begin transferring energy from high to low frequencies. S_{nl} fields already show positive lobes at low frequencies and negative lobes at higher frequencies, indicating energy transfer from wind-sea into the swell band. This is the onset of spectral downshift as cyclonic winds begin to force short waves that are nonlinearly transferred to longer periods.

Figures 7, 8 and 9 shows the increasing spectral energy and stronger S_{nl}, progressive shift of spectral peak to lower frequencies and gradual change from bimodal to unimodal spectra as cyclone-generated long-period energy grows and dominates. Spectral energy and S_{nl} magnitudes increase as the cyclone intensifies. The S_{nl} panels show stronger positive contributions at low frequencies and stronger negative lobes at higher frequency, a clear signature of nonlinear redistribution (quadruplet interactions) that feeds long-period swell energy. During landfall (Fig. 10b-c), the unimodal, low-frequency swell becomes most prominent (local wind-sea peak largely weakened at the track location); swell peak broadens. S_{nl} remains active and the swell peak is broadened which shows a clear outcome of both wind-sea to swell transfer and the swell–swell interactions that redistribute energy within the low-frequency band and further broaden the swell peak. Post landfall (Fig. 10d), the spectra shift back toward higher frequencies and bimodality reappears, consistent with decay of the cyclone forcing and shows relative role for shorter wind-sea components and remote swells again.

In addition to the transfer of wind-sea to swell, via S_{nl}, the panels show evidence that swell–swell interactions, i.e. between TC swells and ETSIO swells (nonlinear exchanges occurring entirely within the low-frequency band) are active as the swell energy builds. These interactions broaden the swell peak and redistribute energy across nearby low frequencies, which helps the low-frequency energy dominate spatially and temporally (Fig. 6d-Fig. 8). Due to this interaction, the swell signal arriving at distant coasts is longer-period, more persistent, and spectrally broader than the initial swell source produced under the cyclone.

5.3 Impact of TC swells in the NIO

In this section, we analyse the effect of tropical cyclone (TC) swells along the coasts. As highlighted in Sections 5.1 and 5.2, high-energy swells are generated and reach the Indian coasts. To further this discussion, the swell attenuation rate was calculated for the target regions, as shown in Fig. 11, indicating that almost 80% of the energy is attenuated before reaching the coast. Spectral analyses were conducted for several coastal locations along the Indian coast, including Kavaratti, Kozhikode, Digha, Gopalpur, Ratnagiri, and Kanyakumari, with representative results for Kavaratti, Kozhikode, and Digha. The model validations with the observations along the coast are shown in Fig. 12 for the representative coastal locations Kavaratti and Kozhikode to prove the reliability of the model. It is evident that the swell energy from the cyclone significantly impacted the coast, particularly from 14th February. According to the propagation patterns, swells reached the Indian coast from Region A by 192 h, consistent with the spectral analysis results. Even though a large portion of the swell energy was attenuated, it still produced a significant impact, as reflected in the spectral analysis with spectral energy density ranging from (0–0.2 m^2/Hz).

Spectral validation was performed using wave-rider buoy data. In Kavaratti, on 21st February at 06:00 UTC, the model data (WW3F spectral distribution) showed good agreement with observations, with only slight underestimations

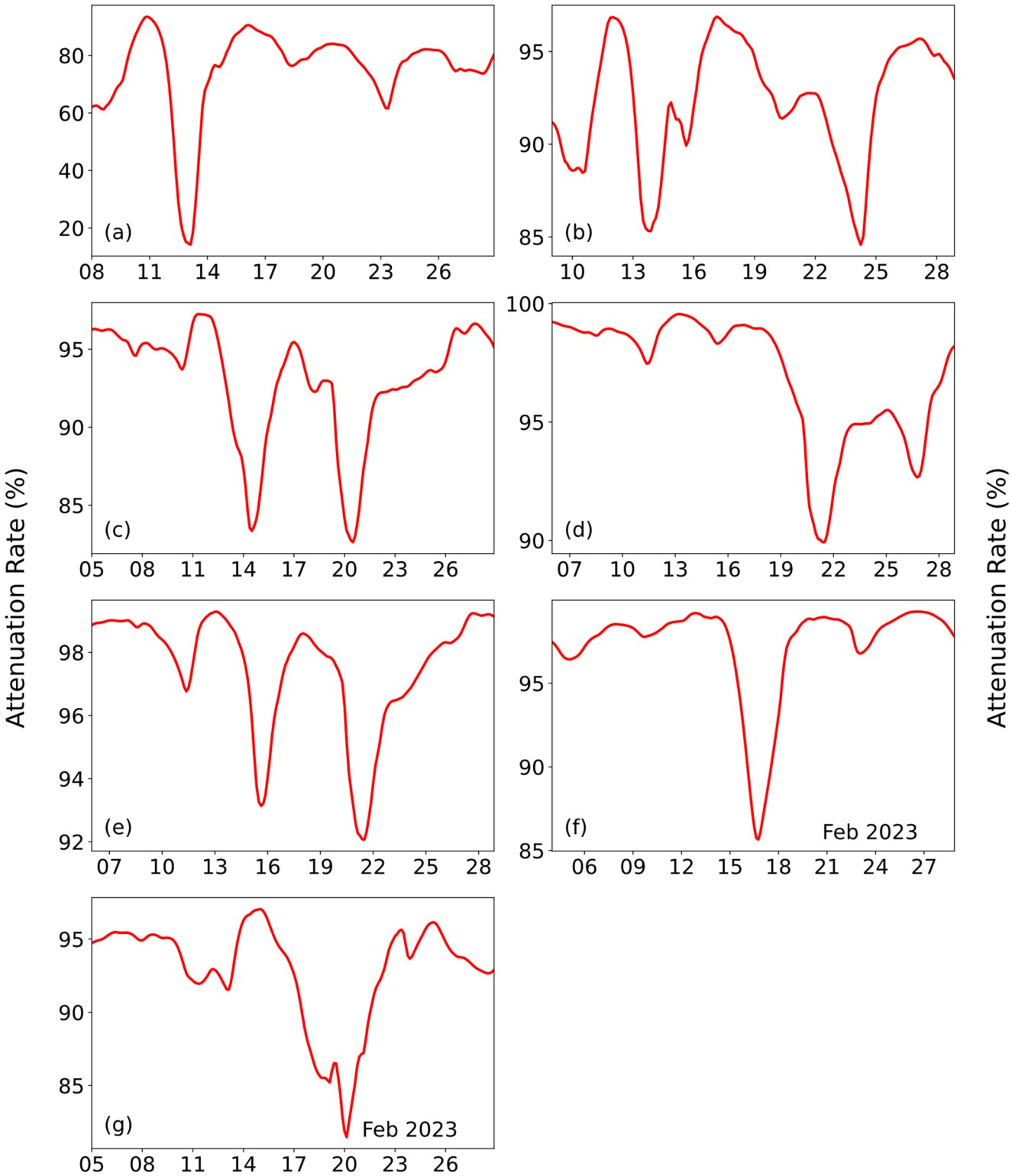

Fig. 11 Rate of attenuation from A-T1 at 168 h (**a**); A-T3 at 192 h (**b**); B-T1 at 96 h (**c**); B-T2 at 120 h (**d**); B-T3 at 120 h (**e**); C-T3 at 72 h (**f**); C-T4 at 96 h (**g**)

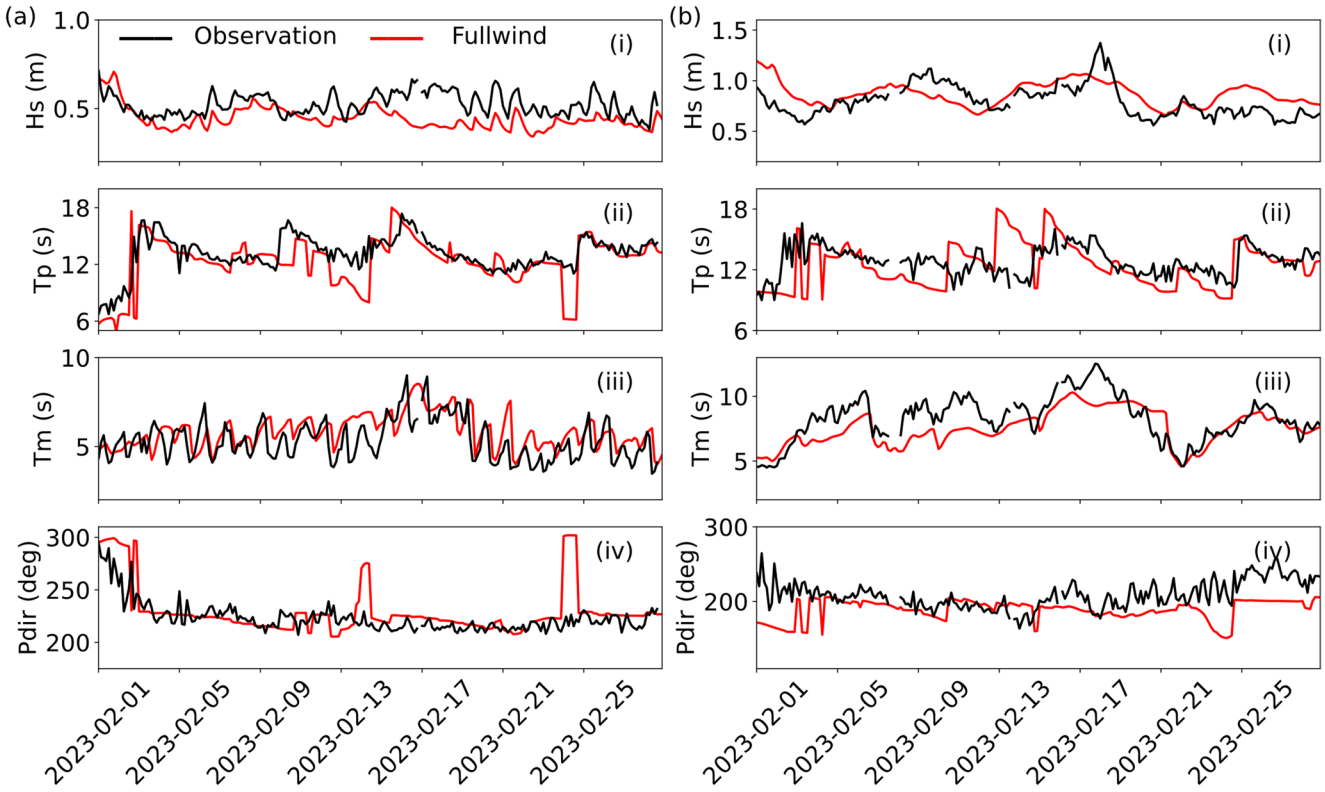

Fig. 12 Validations of the model data WW3F runs with wave buoy data for the locations (**a**) Kozhikode (**b**) Kavaratti

(Fig. 13a). Figure 13b shows Digha on 23rd February at 12:00 UTC, where the model slightly overestimates low-frequency components and underestimates high-frequency components, though it follows the bimodal distribution pattern closely. Figure 13c presents Kozhikode on 21st February at 06:00 UTC, showing strong coherence between model data and observations despite minor mismatches.

The analysis indicates a combined impact of TC swells and ETSIO swells along the coast. To gain a comprehensive understanding of how swells from similar TCs affect the coast and to identify the most affected regions, the wave power density (WPD, kW/m) along the coast up to 500 m depth was filtered and categorized using WW3TC and WW3F runs for the NIO region, as shown in Fig. 14a and b.

From the WW3TC runs (Fig. 14a), the most affected regions along the Indian coast are the southern tip (WPD 0.5–1 kW/m) and the southern coast of Sri Lanka (WPD 0.75–1 kW/m). The eastern coast is generally more affected than the western coast, with most regions experiencing a WPD of 0.25–0.5 kW/m, whereas the Kerala and Karnataka coasts are affected with WPDs of 0.25–0.5 kW/m, and higher energies (0.5–1 kW/m) reach the southern Kerala coast. Island regions are also impacted significantly, with WPDs ranging from 0.5 to 2 kW/m. Also it is evident that the island shadowing effect due to the Srilanka has shielded the southeastern coasts. The northwestern coast of India where the shelf width is high shows less WPD and indicate the swell attenuation in the area compared to southwestern coast which receives direct swell energy. Overall, the analysis shows that swells from TC Freddy strongly affect the southern coast, Sri Lanka, and nearby island regions.

Figure 14b shows WPD along the coast using WW3F runs. In this scenario, coasts experience higher energies due to the combined effects of wind and SIO swells, with WPD exceeding 1.75 kW/m along coasts and islands. The general wave energy characteristics along the Indian coasts during February align well with previous observations (Mithun et al. 2025). Therefore, the effect of TC Freddy along the coast is significant. Although the contribution from WW3TC is less than that from WW3F, these swells generate high wave energies along the NIO coasts and islands, which could lead to adverse impacts.

6 Summary and conclusion

This study emphasizes the wave fields induced by TC Freddy, which persisted for 36 days, supported by atmospheric and oceanic conditions favourable for sustained convection. Although the impact of the ETSIO swells along the various coasts is extensively studied, the swell propagation pattern due to the wavefields due to the TC along the

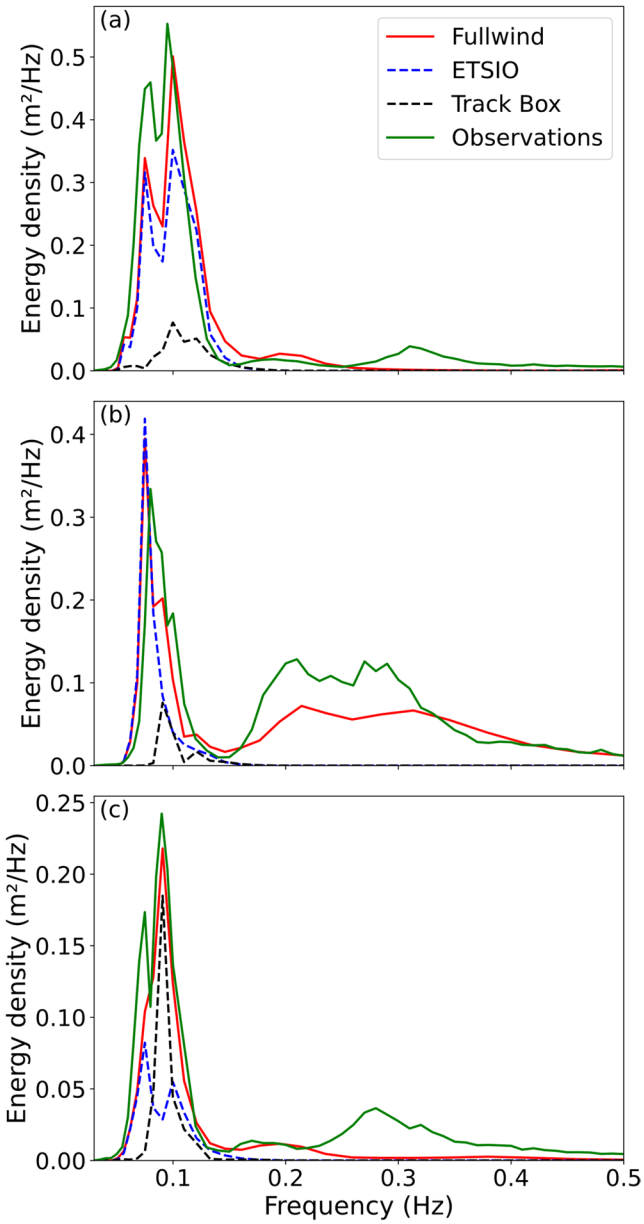

Fig. 13 Spectral validation at (**a**) Kavaratti on 21 February at 06:00, (**b**) Digha on 23 February at 12:00, and (**c**) Kozhikode on 21 February at 06:00

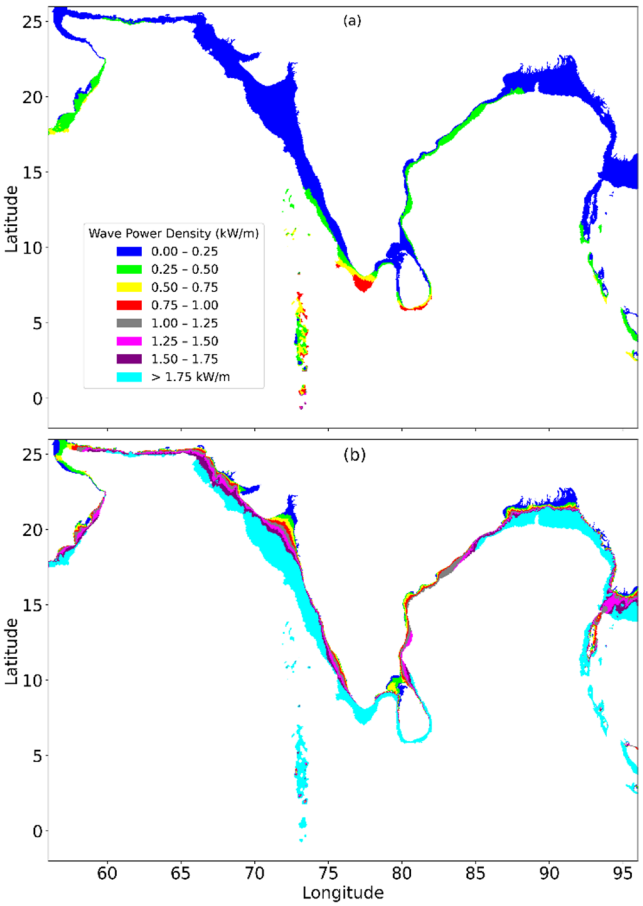

Fig. 14 Wave power density (WPD, kW/m) along the coast within the 500 m depth contour, averaged over 14–28 February 2023 (**a**) WW3TC runs and (**b**) WW3F runs

TSIO is least explored, thus understanding the effects of the TC wavefields along the IO region is very crucial especially for a long lived cyclone like TC Freddy which traversed the entire SIO. The primary objective of the study is to understand the swell propagation patterns and identify the regions most affected by the cyclone.

Analysis of the swell propagation patterns indicates that swells generated by a long-lived cyclone like TC Freddy can propagate across the entire Indian Ocean, reaching the coasts of India, the Gulf region, eastern Africa, and surrounding areas. Moreover understanding the swell propagation pattern provides insights during futuristic situation, not only during a longer cyclone like Freddy, but during various other situations also as the study analyses the impact from various regions across the IO.

Further examination of the 1D spectra and nonlinear interactions along points of the TC track reveals that as the cyclone intensifies, energy in the low-frequency range increases significantly, exceeding contributions from ETSIO swells. During this phase, the peak frequency shifts toward lower frequencies, and the spectral shape becomes unimodal as the cyclone-driven winds dominate the low-frequency swells, preventing the establishment of a distinct secondary peak. The nonlinear interactions support these findings with enhanced positive contributions along the low frequency part and stronger negative lobes at higher frequencies, highlighting the role of quadruplet non-linear interactions leading to the redistribution of energy towards long period swells. The 1D-spectral energy density ranged from approximately 2 to 200 m^2/Hz representing the multiple intensification stages from the period of cyclone genesis to the first landfall. As the cyclone weakens, the spectral shape transitions toward a bimodal distribution, reflecting

contributions from both TC and ETSIO swells at different frequencies with a maximum spectral density of about $5\,m^2/Hz$.

Swell attenuation analysis using WW3TC along the coasts shows that the Indian coasts were not heavily impacted by TC Freddy, with swells losing up to 80% of their energy before reaching the shore. Consequently, only lower wave energies (<2 kW/m) were observed along the coasts, in contrast to the higher energies seen in the general WW3F scenario along the NIO coasts and islands. The most affected regions were the southern tip of India and the southwestern coasts of Kerala with a WPD of (0.5–1.5 kW/m). The southern coast of Srilanka was similarly impacted with WPD of (0.75–1.75 kW/m). The Lakshadweep Islands, Maldives, Srilanka are the greatly affected regions with a WPD of (0.5 −2 kW/m). Thus the regions most affected were the southern coastal areas and nearby islands, suggesting that similar high-energy conditions may occur along these regions during future cyclones of comparable intensity.

This study provides valuable insight into swell propagation patterns and identifies regions along the NIO that are most susceptible to potentially destructive wave impacts during similar cyclonic events. The use of the high resolution unstructured WW3 enabled better understanding the coastal dynamics and the effects along the coasts. Understanding these patterns is essential for anticipating more severe future extremes and developing effective coastal protection strategies to mitigate the impacts of such events.

Acknowledgements This research falls under OCCAS-Deep Ocean Mission, MoES, Govt. India. We thank the developers of WAVEWATCH III NOAA/NCEP for providing the WAVEWATCH III source code (https://polar.ncep.noaa.gov/waves/) and for their consistent efforts to improve the accuracy of this open-source spectral model. This article is also a part of Roshyal Joy's doctoral research and acknowledges the financial support through the Ministry of Earth Sciences (MoES, Govt. of India) "*DEvelopment of SKilled Manpower in Earth Sciences (DESK)*" Research Fellow Program.We thank Dr. Francis P A, Head OMDA and Dr. Girishkumar M S, Scientist, INCOIS, for their support. We also thank the Observation, Data management and ICT divisions of INCOIS for their support. The wave model experiments are performed in MIHIR HPC. This is INCOIS contribution no. 608.

Author contributions RJ: Software, Methodology, Formal analysis, Writing – Original draft, RPG: Writing – Original draft, Methodology, Conceptualization, Formal analysis, BPK: Writing – review & editing, RSM: Data curation TMB: Writing – review & editing.

Funding Funding for this work was provided from the "Deep Ocean Mission" programme of the Ministry of Earth Sciences, Government of India.

Data availability No datasets were generated or analysed during the current study.

Declarations

Competing interests The authors declare no competing interests.

Clinical trial number Not applicable.

References

Ardhuin F, Chapron B, Collard F (2009) Observation of swell dissipation across oceans. Geophys Res Lett. https://doi.org/10.1029/2008GL037030

Balakrishnan NTM, Anoop TR, Arun N et al (2025) WAve monitoring along nearshore (WAMAN) buoy network: best practices and applications in sea state monitoring and forecasting for the Indian ocean. Bull Am Meteorol Soc. https://doi.org/10.1175/BAMS-D-23-0263.1

Bhowmick SA, Kumar R, Chaudhuri S, Sarkar A (2011) Swell propagation over Indian ocean region

Bister M, Emanuel KA (2002) Low frequency variability of tropical cyclone potential intensity 2. Climatology for 1982–1995. J Geophys Research: Atmos. https://doi.org/10.1029/2001JD000780. 107:

Briegel LM and FWM (1997) Large-scale influences on tropical cyclogenesis in the Western North Pacific. Mon Weather Rev 125:1397–1413

Camargo SJ, Emanuel KA, Sobel AH (2007) Use of a genesis potential index to diagnose ENSO effects on tropical cyclone genesis. J Clim 20:4819–4834. https://doi.org/10.1175/JCLI4282.1

Davison S, Benetazzo A, Barbariol F et al (2024) Characterization of extreme wave fields during Mediterranean tropical-like cyclones. Front Mar Sci. https://doi.org/10.3389/fmars.2023.1268830

Deshpande M, Singh VK, Ganadhi MK et al (2021) Changing status of tropical cyclones over the north Indian Ocean. Clim Dyn 57:3545–3567. https://doi.org/10.1007/s00382-021-05880-z

Emanuel KA (1988) The maximum intensity of hurricanes. J Atmos Sci 45:1143–1155

Ghanavati M, Young I, Kirezci E et al (2023) An assessment of whether long-term global changes in waves and storm surges have impacted global coastlines. Sci Rep 13:11549. https://doi.org/10.1038/s41598-023-38729-y

Gray WM et al (1975) Tropical cyclone genesis. Colorado State University Libraries

Grossmann-Matheson G, Young IR, Meucci A, Alves JH (2024) Global tropical cyclone extreme wave height climatology. Sci Rep 14(1):4167. https://doi.org/10.1038/s41598-024-54691-9

Hasselmann K (1963) On the non-linear energy transfer in a gravity-wave spectrum. Part 3. Evaluation of the energy flux and swell-sea interaction for a neumann spectrum. J Fluid Mech 15:385–398

Hasselmann K, Barnett TP, Bouws E et al (1973) Measurements of wind-wave growth and swell decay during the joint North sea wave project (JONSWAP). Ergaenzungsheft zur Deutschen Hydrographischen Zeitschrift, Reihe A

Hersbach H, Bell B, Berrisford P et al (2020) The ERA5 global reanalysis. Q J R Meteorol Soc 146:1999–2049. https://doi.org/10.1002/qj.3803

Klotzbach PJ, Wood KM, Schreck CJ et al (2022) Trends in global tropical cyclone activity: 1990–2021. Geophys Res Lett. https://doi.org/10.1029/2021GL095774

Knutson TR, Sirutis JJ, Zhao M et al (2015) Global projections of intense tropical cyclone activity for the late twenty-first century

from dynamical downscaling of CMIP5/RCP4.5 scenarios. J Clim 28:7203–7224. https://doi.org/10.1175/JCLI-D-15-0129.1
Kossin JP, Knapp KR, Olander TL, Velden CS (2020) Global increase in major tropical cyclone exceedance probability over the past four decades. Proc Natl Acad Sci U S A 117:11975–11980. https://doi.org/10.1073/pnas.1920849117
Kumar R, Bhowmick SA, Ray S et al (2009) Improvement in predictability of waves over the Indian ocean. Nat Hazards 49:275–291. https://doi.org/10.1007/s11069-008-9310-y
Mithun SB, Remya PG, Sreejith M et al (2025) Assessment of ocean wave energy potential and identification of technologically feasible hotspots for Indian coastal regions. J Ocean Eng Mar Energy. https://doi.org/10.1007/s40722-025-00407-8
Paul D, Panda J, Routray A (2022) Ocean and atmospheric characteristics associated with the cyclogenesis and rapid intensification of NIO super cyclonic storms during 1981–2020. Nat Hazards 114:261–289. https://doi.org/10.1007/s11069-022-05389-6
Peduzzi P, Chatenoux B, Dao H et al (2012) Global trends in tropical cyclone risk. Nat Clim Chang 2:289–294. https://doi.org/10.1038/nclimate1410
Perry Z, Rapolaki R, Roffe S, Ragoasha M (2024) Analysing the atmospheric-oceanic conditions driving the sustained long track and intensity of tropical cyclone Freddy. Trop Cyclone Res Rev 13:356–388. https://doi.org/10.1016/j.tcrr.2024.11.008
Raj A, Kumar BP, Remya PG et al (2023) Assessment of the forecasting potential of WAVEWATCH III model under different Indian ocean wave conditions. J Earth Syst Sci 132:32. https://doi.org/10.1007/s12040-023-02045-w
Ramakrishnan R, Remya PG, Mandal A et al (2022) Wave induced Coastal flooding along the Southwest Coast of India during tropical cyclone Tauktae. Sci Rep 12:19966. https://doi.org/10.1038/s41598-022-24557-z
Reboita MS, da Rocha RP, Ambrizzi T, Gouveia CD (2015) Trend and teleconnection patterns in the climatology of extratropical cyclones over the Southern hemisphere. Clim Dyn 45:1929–1944. https://doi.org/10.1007/s00382-014-2447-3
Remya PG, Vishnu S, Praveen Kumar B et al (2016) Teleconnection between the North Indian ocean high swell events and meteorological conditions over the Southern Indian ocean. J Geophys Res Oceans 121:7476–7494. https://doi.org/10.1002/2016JC011723
Roberts KJ, Pringle WJ, Westerink JJ (2019) OceanMesh2D 1.0: MATLAB-based software for two-dimensional unstructured mesh generation in coastal ocean modeling. Geosci Model Dev 12:1847–1868
Sabique L, Annapurnaiah K, Balakrishnan Nair TM, Srinivas K (2012) Contribution of Southern Indian ocean swells on the wave heights in the Northern Indian ocean—a modeling study. Ocean Eng 43:113–120. https://doi.org/10.1016/j.oceaneng.2011.12.024
Samiksha SV, Vethamony P, Aboobacker VM, Rashmi R (2012) Propagation of Atlantic Ocean swells in the North Indian ocean: a case study. Nat Hazards Earth Syst Sci 12:3605–3615. https://doi.org/10.5194/nhess-12-3605-2012
Sebastian M, Behera MR (2015) Impact of SST on tropical cyclones in North Indian ocean. Procedia Eng 116:1072–1077. https://doi.org/10.1016/j.proeng.2015.08.346
Shimura T, Mori N, Mase H (2015) Future projections of extreme ocean wave climates and the relation to tropical cyclones: ensemble experiments of MRI-AGCM3.2H*. J Clim 28:9838–9856. https://doi.org/10.1175/JCLI-D-14-00711.1
Singh, O. P. (2010). Recent Trends in Tropical Cyclone Activity in the North Indian Ocean. In Indian Ocean Tropical Cyclones and Climate Change (pp. 51–54). Springer Netherlands. https://doi.org/10.1007/978-90-481-3109-9_8Singh
Sreelakshmi S, Bhaskaran PK (2022) Extreme swell wave energy and its directional characteristics in the Indian Ocean. Clim Dyn 58:2193–2212. https://doi.org/10.1007/s00382-021-06000-7
Sreelakshmi S, Bhaskaran PK (2023) Swell wave propagation and its characteristics while approaching the Indian Coast. Clim Dyn 60:1271–1295. https://doi.org/10.1007/s00382-022-06378-y
Susilo A, Perrie W, Toulany B (2017) On quadruplet interactions for ocean surface waves
Tamizi A, Young IR (2020) The spatial distribution of ocean waves in tropical cyclones. J Phys Oceanogr 50:2123–2139. https://doi.org/10.1175/JPO-D-20-0020.1
Tolman HL (2009) User manual and system documentation of WAVEWATCH III TM version 3.14. Technical Note, MMAB Contribution 276(220)
Ussalu JLM, Manjate GMA (2024) Climate systems behind the observed singularities of the very intense tropical cyclone FREDDY
Walsh EJ, Wright CW, Vandemark DC et al (2000) Hurricane directional wave spectrum spatial variation in open ocean and at landfall. In: IGARSS 2000. IEEE 2000 International Geoscience and Remote Sensing Symposium. Taking the Pulse of the Planet: The Role of Remote Sensing in Managing the Environment. Proceedings (Cat. No.00CH37120). IEEE, pp 2750–2752
Wu L, Sahlée E, Nilsson E, Rutgersson A (2024) A review of surface swell waves and their role in air–sea interactions. Ocean Model 190:102397. https://doi.org/10.1016/j.ocemod.2024.102397
Wu L, Zhang H, Chen J-M, Feng T (2020) Characteristics of tropical cyclone activity over the South China sea: local and nonlocal tropical cyclones. Terr Atmospheric Ocean Sci 31:261–271. https://doi.org/10.3319/TAO.2019.07.01.02
Zheng C, Wu D, Wu H et al (2022) Propagation and attenuation of swell energy in the Pacific Ocean. Renew Energy 188:750–764. https://doi.org/10.1016/j.renene.2022.02.071
Zheng CW, Li CY, Pan J (2018) Propagation route and speed of swell in the Indian ocean. J Geophys Res Oceans 123:8–21. https://doi.org/10.1002/2016JC012585